Energy Technology
Generation, Conversion, Storage, Distribution
www.entechnol.de

Energy, Exergy, Economic and Exergoeconomic Analyses of Chemical Looping Combustion Plant Using Waste Bark for District Heat and Power Generation with Negative Emissions

Gajanan Dattarao Surywanshi, Henrik Leion, and Amir H. Soleimanisalim*

The greenhouse gas emissions from the boiler of pulp and paper industries can be minimized by adapting chemical looping combustion (CLC) technology. This work aims to analyze the energy, exergy, economic, and exergoeconomic performance of an industrial scale CLC plant for district heat and electricity generation using waste bark from the paper and pulp industry. The CLC plant with one natural ore and one industrial waste oxygen carrier (OC) is modeled using Aspen Plus. The performance of the CLC plant has been compared to Örtofta combined heat and power plant without CO_2 capture and with post-combustion CO_2 capture as the reference cases. Results showed that the CLC-based power plant is energetically, exegetically, and economically efficient compared to the reference cases. The circulating fluidized bed boiler unit contributes the highest exergy destruction (about 50–80%). Among the CO_2 capture plants, the CLC plant with ilmenite has the lowest levelized cost of district heat (4.58 € GJ^{-1}), and a payback period (9.69 years) followed by the CLC plant with LD slag (5.91 € GJ^{-1} and 11.84 years), and the plant with PCC (6.94 € GJ^{-1} and 13.58 years). The exergoeconomic analysis reveals that the CLC reactors have the highest cost reduction potential, followed by the steam turbine.

1. Introduction

Paper and pulp industries are, and have long been, significant parts of the Swedish economy.[1] These industries in Sweden play a vital role in the biomass supply chain and account for about 50% of the total energy use in the country.[2] The Swedish paper and board industry consists of 41 paper mills and 41 pulp mills[3] and produced 10.10 Mton market pulp and 8.90 Mton paper and board in 2021. Sweden is the largest pulp producer and the third largest producer of paper in Europe.[4] The pulp and paper industry is highly energy-intensive and accounts for 45% of the industrial utilization of fuel and electricity in Sweden and emits about 22.84 Mton of CO_2 emission per year.[5] However, even with increased demand for paper products, the pulp and paper industry must reduce its greenhouse gas emissions to meet the United Nations' (UN) goal to limit the global rise in temperature below 1.5 °C.[6] The pulp and paper sector utilizes biomass residues in the boilers as a primary energy source for the internal use of heat and electricity. Although biomass fuels are considered carbon-neutral, the paper and pulp industries can achieve net negative CO_2 emissions by the implementation of carbon capture and storage (CCS) systems on combustion boilers.[7] Hence, the possible approaches using CO_2 removal technology that can achieve negative emissions play an important role in meeting this target.

One effective strategy for reducing CO_2 emissions from the power sector is to recover possible residual heat.[8] The residual or excess heat can be internally used in the other processes to reduce primary energy usage and it can also be used externally in the form of district heat. The adaption of the district heating network in Sweden has significantly decreased CO_2 emissions from the heating sector.[9] The utilization of excess heat for district heating is generally considered emissions-free or CO_2-free.[10] Studies reported that further expansion of the district heating network could reduce cost and CO_2 emissions in the European Union (EU) energy system.[11,12] About 71% of the urban district heating demand can be met in 14 analyzed EU member states, of which about 78% of total district heat demand can be supplied by the residual heat from the power plants.[13]

The industrial residual heat can also be utilized by CCS processes. CCS plays an important role in limiting global warming by enabling CO_2 emissions reduction by retrofitting the existing plants.[14] After applying CCS to biomass fuel-based thermal

G. D. Surywanshi, H. Leion
Department of Chemistry and Chemical Engineering
Chalmers University of Technology
41293 Gothenburg, Sweden
E-mail: dattarao@chalmers.se

A. H. Soleimanisalim
Biorefinery and Energy
RISE Research Institutes of Sweden
Gothenburg 41279, Sweden

The ORCID identification number(s) for the author(s) of this article can be found under https://doi.org/10.1002/ente.202300577.

DOI: 10.1002/ente.202300577

power plants, net "negative emissions" can be achieved. The conventional way of CO_2 capture processes (pre-combustion, post-combustion, and oxy-combustion) utilize a considerable amount of heat and/or electricity from the plant.[15] The utilization of this heat ultimately reduces the overall energy efficiency of the plant. The energy penalty for the pre-combustion capture process is between 7% and 10%,[16,17] for the post-combustion capture (PCC) process, the energy penalty is between 8% and 12%,[18,19] and for the oxyfuel combustion capture process, the energy penalty is between 9.50% and 12.00%.[20,21] Thus, a new strategy for carbon capture is needed to reduce overall CO_2 emissions and reduce the use of excess heat for CCS processes.[22]

Chemical looping combustion (CLC) is a promising technology for the combustion of a variety of fuels, including solid biomass, with inherent CO_2 capture.[15] CLC technology is often superior to other alternatives with respect to thermal efficiency and has a good potential to achieve negative CO_2 emissions for the thermal conversion of fuels.[23] CLC uses metal oxides (Me_xO_y) as an oxygen carrier (OC), which is circulated between the two reactors, air, and fuel reactors (**Figure 1**). The combustion of fuel or reduction of OC(Me_xO_y to Me_xO_{y-1}) occurs in the fuel reactor (FR) and oxidation or re-oxidation of reduced OC (Me_xO_{y-1} to Me_xO_y) occurs in the air reactor (AR). These reactions are shown below in reaction (1) and (2). As fuel is combusted in FR without mixing with air, the flue gas stream leaving FR is comprised of mainly steam and CO_2. The CO_2 can be separated by condensing steam avoiding the use of PCC.[24] The OC can be Cu-based, Ni-based, Co-based, Fe-based, Mn-based, or combinations of several metal oxides.[25]

$$\text{Fuel} + MeO \rightarrow Me + H_2O + CO_2 \quad (1)$$

$$Me + 0.5\,O_2 \rightarrow MeO \quad (2)$$

CLC studies have focused on the lifetime of metal oxide particles, combustion efficiency, chemical kinetics, material stability, and economic analysis.[25,26] The different fuel-based (i.e., syngas, biomass, natural gas, coal, etc.) CLC power plants have a net energy efficiency ranging from 35% to 46%, with negligible CO_2 emissions.[27–30] The LCOE for CLC-based power plants was estimated between 88 and 127 \$ MWh^{-1}.[15,28] One of the major issues of the thermal conversion of biomass is the high alkali content of biomass compared to other solid fuels. The alkali can cause corrosion or be deposited in the downstream equipment like heat exchangers or pipes (lowering their efficiencies and causing blockage) or causing agglomeration in the bed material.[31] However, the OC in CLC acts as an alkali scavenger and the gaseous stream from AR in CLC has less alkali compared to FR; therefore, less flue gas cleaning is needed compared to the traditional combustion.[32]

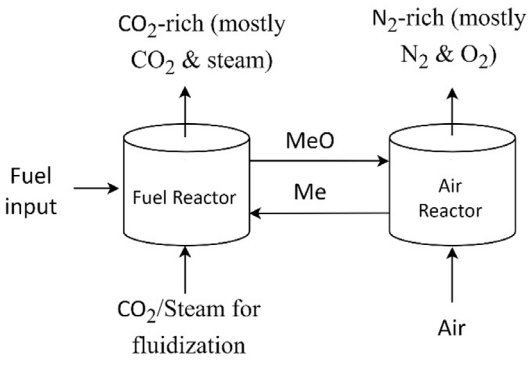

Figure 1. Chemical looping combustion system.

Integration of CLC technology with the bark-fired boiler can have huge potential to achieve negative CO_2 emission in the thermal conversion of bark, one of the main byproducts of paper and pulp industries. However, the implementation of bark in the CLC process in the pulp and paper sector and its greenhouse gas (GHG) emission savings have not yet been investigated. The use of a CLC-based circulating fluidized bed (CFB) boiler instead of a conventional CFB boiler can reduce the ash deposition problem in downstream equipment.[33] This can be a huge advantage when the bark is used as it has high alkali content, high water content, and lower heating value compared to solid fossil fuel.[7] To date, many researchers have worked experimentally and theoretically on CLC-based power plants. **Table 1** shows the compilation of different works on performance assessment of CLC plants in the literature based on the method of evaluation, OC used, coal type, and plant type. Surywanshi et al.[15] compared CLC plants for different steam generation technologies (subcritical, supercritical, and ultrasupercritical) based on thermodynamic and economic analyses. The supercritical CLC plant is found to be the most favorable choice with 89.05 € MWh^{-1} of cost of electricity and 39.77 € t^{-1} of CO_2 avoided cost. A comprehensive review of energy and exergy analyses of steam power plants is given by Khaleel et al.[34] and the 4-E (energy, exergy, economic, and exergoeconomic) analyses of thermal power plant is given by R. Kumar.[35] Their review work suggested that there is a scope for performing different analyses for direct comparisons of different thermal power plants.

Limited research on the thermoeconomic or the exergoeconomic analysis of CLC-based plants is found in the literature. The exergoeconomic analysis is the combination of exergy and economic analysis. This analysis assists in evaluating and optimizing the performance of the plant by considering the inefficiencies (exergy destruction) of an individual unit in the plant and the costs associated with these inefficiencies.[36] Therefore, the exergoeconomic analysis is a next-stage evaluation method of the energy conversion system primarily focused on the cost rates of exergy destruction and exergy. This analysis has been effectively applied to the power generation system[37] and combined heating, cooling, and power generation systems.[38] Khan and Shamim[39] investigated the exergoeconomic analysis of chemical looping reforming (CLR) for H_2 production and concluded that the CLR and heat recovery steam generation units are the most vital units.

To the best of our knowledge, no research has been conducted on the integration of CLC with waste bark-fired boilers in paper and pulp industries for district heat and power generation and its performance comparison with conventional plant (Örtofta) without/with PCC based on energy, exergy, economic and exergoeconomic analysis. Therefore, this study contributes to filling this gap and provides potential technical feasibility and theoretical understanding of the plant with district heat and electricity generation. The main objective of this work is to study the

Table 1. Performance comparison of CLC plants in the literature.

Plant type	Fuel, MW [LHV/HHV]	Oxygen carrier	Net energy efficiency [%]	CO_2 capture efficiency [%]	Performance evaluation basis	Source
IGCC-CLC	27.11 (HHV)	NiO	31.50	100.00	Energy analysis	[61]
					Economic analysis	
iG-CLC	27.14 (HHV)	MoO_3	39.38	96.83	Energy analysis	[62]
					Exergy analysis	
CDCL	26.81 (LHV)	Fe_2O_3	59.98	100.00	Energy analysis	[63]
CDCL	30.53 (HHV)	Fe_2O_3	39.70	100.00	Energy analysis	[64]
					Exergy analysis	
iG-CLC	30.53 (HHV)	NiO	58.20	≈100.00	Energy analysis	[65]
					Exergy analysis	
IGCC-CLC	27.80 (LHV)	NiO	53.19	99.97	Energy analysis	[66]
					Ecological analysis	
					Economic analysis	
iG-CLC	16.25 (LHV)	Fe_2O_3	39.00	88.90	Energy analysis	[67]
		TiO_2	40.54	90.63		
iG-CLC	16.25 (LHV)	$FeTiO_3$	39.00	89.05	Energy analysis	[29]
	`21.88 (LHV)		46.00	88.07	Ecological analysis	
	26.45 (LHV)		44.00	88.36		
IGCC-CLC	22.30 (HHV)	Fe_2O_3/NiO	35.90–46.80	≈100.00	Energy analysis	[68]
	31.90 (HHV)				Economic analysis	
IGCC-CLC	16.72 (HHV)	NiO	40.20	99.97	Energy analysis	[69]
					Exergy analysis	

CLC plant with district heat and electricity generation using two different OCs (ilmenite and LD slag) with waste bark from the paper and pulp industry as a primary energy input to the plant. The overall performance of the CLC-based power plants is compared with each other and PCC plants based on energy, exergy, and, economic analysis. The exergoeconomic analysis is also carried out for CLC plants for both OCs. The results obtained from this work can help to identify investment cost and exergetic destruction and offer possible measures to improve process parameters. In addition, a conventional plant with PCC is also modeled to compare it with the CLC plants. The comprehensive analysis of energy, exergy, economic, and exergoeconomic provides the direct comparison of the CLC plant with the base and PCC plants and, hence, plays a key role in selecting suitable technology to enhance heat and power in the paper and pulp industries.

2. Methodology

In this work, a steady-state simulation using Aspen Plus v12.1,[40] a chemical process simulation environment, has been used for the modeling of the power plant. The Swedish site Örtofta with a district heat and power generation plant operated by the company Kraftringen Energi has been considered as a base or reference plant and the results are validated by Björnsson et al.[41] A PCC technique is integrated with the modeled base plant. This base plant is then modified by replacing a conventional combustor with a CLC unit with different configurations. The modeling results of air and fuel reactors of the CLC system have been validated with results given by Sikarwar et al.[24] This work focuses on evaluating the effect of CLC integration using waste bark from the paper and pulp industry for two OCs and comparison with the base plant. Thus, the following four cases have been considered in this study:

Case – 1: Base plant without CO_2 capture.
Case – 2: Plant with post-combustion capture.
Case – 3: Plant with CLC using ilmenite as an OC.
Case – 4: Plant with CLC using LD slag as an OC.

A waste-bark, whose characteristics are given in **Table 2**, with an energy input of 30 MW_{th} is fed to all power plant cases. The two OCs—ilmenite ore, and LD slag are considered in CLC plants as given in Table 2. The ilmenite ore is considered a benchmark OC and LD slag, which is a waste by-product from Swedish-Finish Steel producers[42] considered an alternative OC. The FeO, Fe_2O_3, and TiO_2 given in **Table 3** are considered OC components in the Aspen simulation, and the remaining are assumed as inert. The Fe-based metal oxide in ilmenite ore is available as FeO, which will convert into Fe_2O_3 after the first redox cycle in the CLC process. Therefore, ilmenite after the first cycle will have a better oxygen transport capacity after one cycle.

2.1. System Description

This section contains a base plant without CO_2 capture, a base plant with PCC, and a CLC-based plant with inherent CO_2 capture. The Örtofta CHP plant was first modeled for the first two

Table 2. Characteristics of waste-bark.[70]

Parameter	Values
Proximate analysis [wt%]	
Moisture	12.5
FC	19,70
VM	77,30
Ash	3,00
Ultimate analysis [wt%]	
C	51,80
H	5,90
N	0,40
Cl	0,00
S	0,04
O	38,86
Calorific value [MJ kg^{-1}]	
LHV	19.60
Exergy based on LHV (Equation (14))	20.98

Table 3. Fresh oxygen carrier composition [wt%].

OC/component	SiO_2	Al_2O_3	FeO	Fe_2O_3	TiO_2	CaO	MgO	Other
Ilmenite[71]	0,36	0,44	42,14	–	50,77	0,13	2,05	4.11
LD slag[42]	14,14	1,20	–	28,84	1,30	42,04	9,10	3.39

cases. The second case involves an additional MEA-based PCC system. Finally, the combustor of the base plant was replaced using air and fuel reactors in the CLC process with an additional CO_2 separator and compressor. The process description of each plant is given as follows:

2.1.1. Base Plant Without CO_2 Capture

The current Örtofta combined heat and power plant connected to the district heat grid is considered a reference or base plant. The model development and process simulation using CHEMCAD software are given in Björnsson et al.[41] This plant is then re-simulated using an Aspen Plus simulation environment and validated with the published results for 30 MW_{th} power input. The simplified process flow diagram of bark-fired base plant without CO_2 capture is shown in **Figure 2**. More information about this case is given in reference case of Björnsson et al.[41]

The base plant consists mainly of a CFB boiler, superheater, FG condenser, DH condenser, steam turbine, compressor, and pumps. The operating conditions for the base plant without CO_2 capture are given in Table 7. The bark (stream 3) is supplied to the CFB boiler at 1.53 kg se^{-1} in the presence of compressed air (stream 2). The sand (stream 4) is added to the CFB boiler to distribute the heat evenly throughout the bed and improve combustion efficiency. The energy from gaseous fuel/flue gas (stream 6) leaving the CFB boiler is extracted in the superheater using pumped water (stream 15) and solid bottom ash is collected at the bottom (stream 5) of the CFB boiler. The water is superheated to 540 °C and 107 bar. The superheater steam (stream 16) is then passed through the steam turbine along with a generator to generate electricity. The steam leaving the steam turbine (stream 17) has some leftover energy which is utilized in the DH condenser. The condensed water (stream 18), along with makeup water (stream 13), is recycled (stream 14) back to the superheater.

As all the energy cannot be extracted from the flue gas (stream 6), the remaining energy from the flue gas leaving the superheater (stream 7) is extracted in the FG condenser with the recycled water from the district heating network (stream 9). The water from the DH network is available at 44 °C[41] and is pumped (stream 10) to the FG condenser, where the maximum

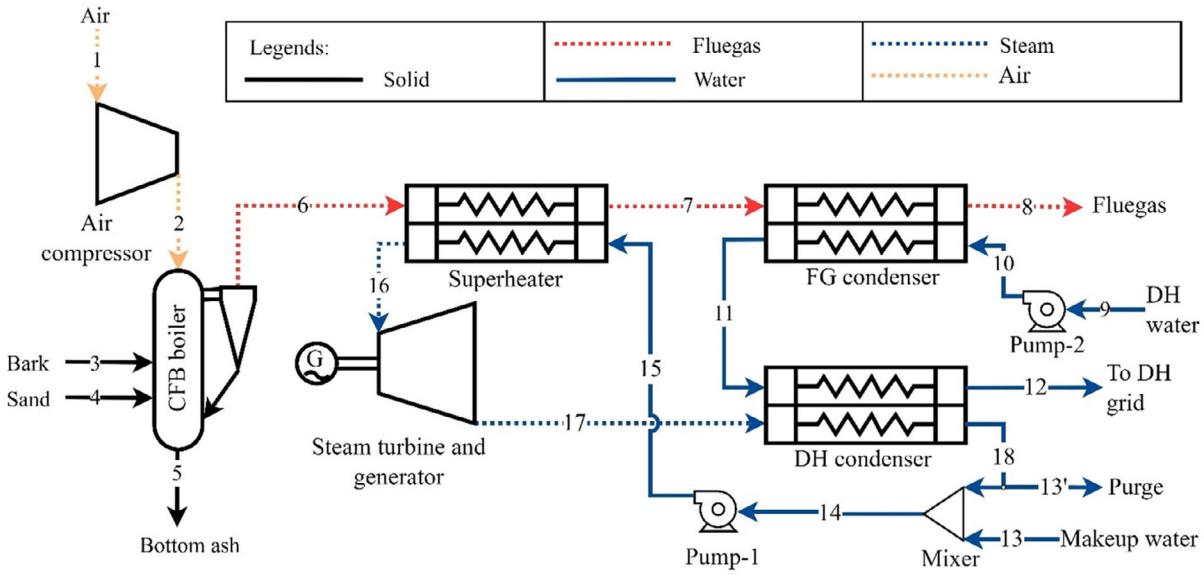

Figure 2. Simplified process flow diagram for the base plant without CO_2 capture for DHP generation.

possible energy is extracted from the flue gas stream. Stream 11 is then passed through the DH condenser to heat to 93.3 °C[41] (stream 12). This hot water stream is connected to the DH grid.

2.1.2. Plant with Post-Combustion Capture

The simplified process flow diagram of the plant with the standard monoethanolamine (MEA) solvent-based regenerative absorption–desorption system for PCC is shown in **Figure 3**. This plant with CO_2 capture consists of all the units present in the base plant without CO_2 capture, in addition, the absorber, stripper, pumps, and CO_2 compressor are included.

The plant with PCC case follows the same process configuration as described in the section 'base plant without CO_2 capture'. The flue gas from the carbon capture process (stream 8 at 50 °C) is sent to the absorber of the PCC process. The aqueous absorbent (MEA) solution enters (stream 19) the absorber countercurrently with the flue gas, where MEA reacts chemically with CO_2. Chemically bonded MEA and CO_2 (stream 21) are pumped to the stripper after passing through the heat exchanger, where it is preheated to a temperature of 120 °C. The solvent regeneration and separation of CO_2 from chemically bonded MEA and CO_2 occurs in the stripper column (130 °C and 2.30 bar). The CO_2 is separated from the top of the column (stream 24), washed and cooled, and then sent to compression. The energy required in the reboiler to regenerate MEA is compensated by the flue gas stream leaving the superheater (stream 7). This use of energy from the power system reduces the overall efficiency of the power plant. The MEA-water mixture is collected from the bottom of the stripper (stream 28) and pumped back to the absorber after cooling it. The CO_2 from the stripper is compressed to 110 bar in the CO_2 compressor (Table 7).

The model for the regenerative absorption-desorption system was initially developed and validated on the pilot plant scale using the data available in the literature.[43] The model parameters were handled using Chemical Engineering design and principles.[44] The preliminary design calculation results and process specifications for the plant are given in **Table 4**. **Table 5** shows the design specifications for the absorber and stripper sections of scaled-up MEA-based PCC.

During the absorption and stripping processes, the equilibrium and kinetic reactions that take place are presented below[45]

$$H_2O + MEAH^+ \leftrightarrow MEA + H_3O^+ \quad (3)$$

$$2H_2O \leftrightarrow H_3O^+ + OH^- \quad (4)$$

$$CO_2 + 2H_2O \leftrightarrow H_3O^+ + HCO_3^- \quad (5)$$

$$HCO_3^- + H_2O \leftrightarrow CO_3^{--} + H_3O^+ \quad (6)$$

$$CO_2 + OH^- \rightarrow HCO_3^- \quad (7)$$

$$HCO_3^- \rightarrow CO_2 + OH^- \quad (8)$$

$$MEA + CO_2 + H_2O \rightarrow MEACOO^- + H_3O^+ \quad (9)$$

$$MEACOO^- + H_3O^+ \rightarrow MEA + H_2O + CO_2 \quad (10)$$

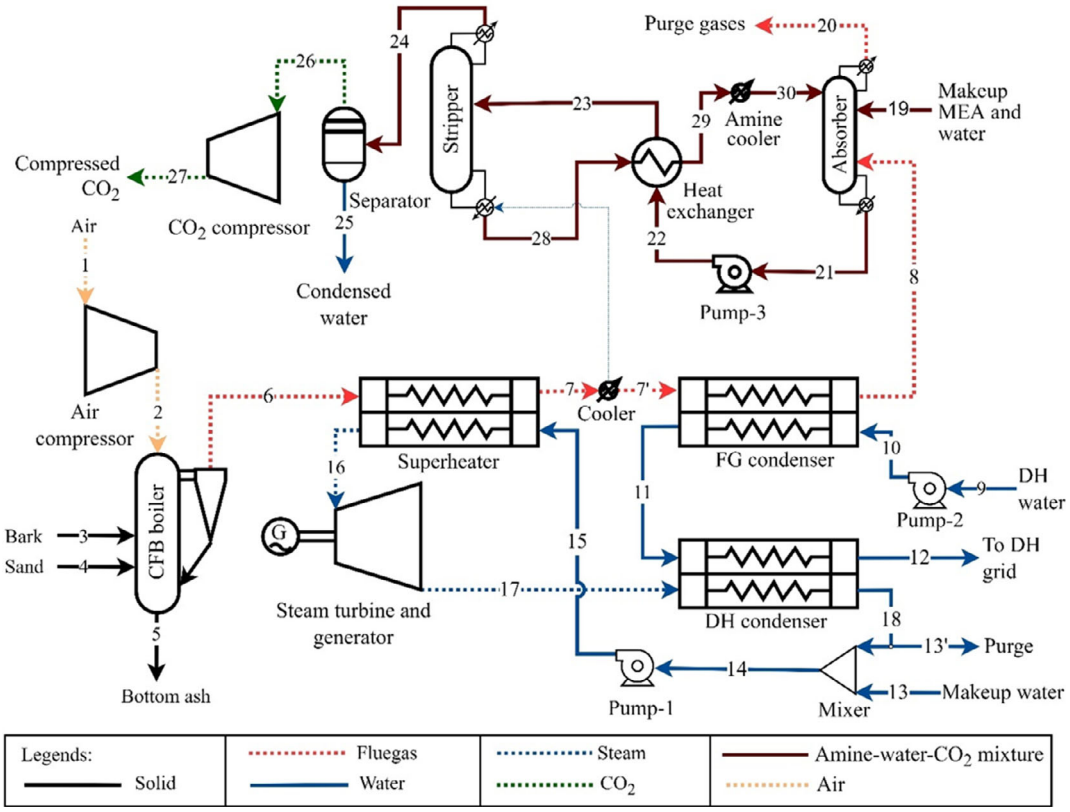

Figure 3. Simplified process flow diagram for a plant with post-combustion CO_2 capture.

Table 4. Assumptions in preliminary design calculation and results for CO_2 separation using MEA at first stage.

Description	Unit	Value
Flow rate of flue gas entering the absorber	$kg\,s^{-1}$	12.41
Flow rate of CO_2 entering the absorber	$kg\,s^{-1}$	2.30
Mass fraction of CO_2 in the flue gas	%	12.26
Required MEA-H_2O flow rate	$kg\,s^{-1}$	39.39
CO_2/MEA mass ratio	–	0.20
Condenser Heat Duty	MW	40.30
Reboiler Heat Duty	MW	46.80

Table 5. Design specification for the full-scale MEA-based PCC absorber and stripper.

Parameter	Absorber	Stripper
Column number	1	1
Calculation type	Rate-based	Rate-based
Number of equilibrium stages	6	6
Condenser	None	Partial-vapour
Reboiler	None	Kettle
Operating pressure [bar]	1.013	1.62
Type of packing	IMTP – NORTON	FLEXIPAC – KOCH
Total height of packing [m]	6	10
Diameter of column [m]	2.5	4

The equilibrium constants for the reactions (1)–(4) were calculated from the standard Gibbs free energy change (DGAQFM). DHAQFM (aqueous heat of formation at infinite dilution) and CPAQ0 (aqueous phase heat capacity at infinite dilution) of $MEAH^+$ and $MEACOO^-$, to calculate the standard $MEAH^+$ and $MEACOO^-$ Gibbs free energy.[43] The kinetic parameters and power law expressions used for the rate-controlled reactions (5)–(8)[46] are listed in **Table 6**.

2.1.3. Plant with Chemical Looping Combustion

The simplified process flow diagram of a CLC-based plant with district heat and power generation is shown in **Figure 4**. The main components of this plant are the CFB boiler (air and fuel reactor coupled together in a loop), superheater, FG condenser, DH condenser, steam turbine, pumps, and compressors. The conventional CFB boiler of the base plant is replaced with air and fuel reactors of the CLC system in the CLC-based plant.

Table 6. Parameters of k_0 and E for the kinetic reactions.[46]

Reaction	k_0	E [cal mol^{-1}]
(5)	4.32×10^{13}	13 249
(6)	2.38×10^{17}	29 451
(7)	9.77×10^{10}	9855.8
(8)	3.23×10^{19}	15 655

In addition, a flash separator is used for the separation of CO_2 from steam instead of the absorber and stripper used in MEA-based CO_2 capture process. Multiple heat exchangers are used for the superheater and FG condenser in the CLC plant instead of a single heat exchanger in the base plant.

Bark (fuel) is fed to the fuel reactor (stream 3) with the recycled OC from the AR (stream 6). The combustion of bark takes place in the fuel reactor in the presence of an OC and 1% OC along with bottom ash is assumed to be purged at the bottom (stream 10) to avoid sintering inside the reactor. It is also assumed that the purged OC is not recovered and the same amount of fresh OC is added to the fuel reactor. The OC is reduced in the fuel reactor and sent to the AR (stream 9) to re-oxidize it in the presence of air (stream 2). The flue gas which is mainly CO_2 and steam from the fuel reactor (stream 8), and oxygen depleted air (900 °C) from the AR (stream 5) are sent to the superheater to extract heat from them. The water is pumped to the superheater (stream 24) at 107 bar and heated to 540 °C in a superheater (stream 25). The high-pressure steam is passed through the steam turbine unit to generate electricity. The remaining heat from FG and DA streams leaving the superheater (streams 11 and 12) is recovered in the FG condenser and the remaining heat from stream 26 is recovered in the DH condenser. The recovered heat using FG and DH condensers is utilized to heat district heating water from 44 °C (stream 18) to 93.3 °C (stream 21). The stream 21 is connected to the district heating network. The CO_2 from the flue gas stream leaving the FG condenser (stream 14) is separated by condensing steam (stream 15) in a flash separator. The CO_2 is then compressed to 110 bar (stream 17).

2.2. Simulation Assumptions

In this work, Aspen Plus v12.1 simulation software[40] is used for the steady-state simulation of the base plant, plant with PCC and CLC plant. The Peng Robinson and Boston Mathias (PR–BM) model is used to determine the physical properties of non-conventional bark, flue gas, OC, and air and STEAM-NBS is used to determine the properties of water and steam.[15] The simulation assumptions and specifications are given in **Table 7**. The process simulation also considers the following assumptions: 1) Steady-state conditions for all the components. 2) Reference environment: 21% O_2% and 79% N_2; ambient temperature: 5.2 °C;[47] ambient pressure: 1.013 bar. 3) Energy input to the plant is assumed to be 30 MW_{th} based on the LHV of bark. 5) Pressure and heat losses are negligible.[48] 4) Temperature difference approach for heat exchangers: 10 °C.[15] 5) Calculation options for CFB boiler (air and fuel reactor in case of CLC plant: chemical and phase equilibrium.[15] 6) Tar and ash are inert substances.[48] 7) Gas–liquid separation is simulated using a Flash module.[48]

2.3. Data Analysis

In this work, the overall performance of all the DHP plants is compared based on energy, exergy, and economic analyses. The exergoeconomic analysis on CLC-based plants with ilmenite

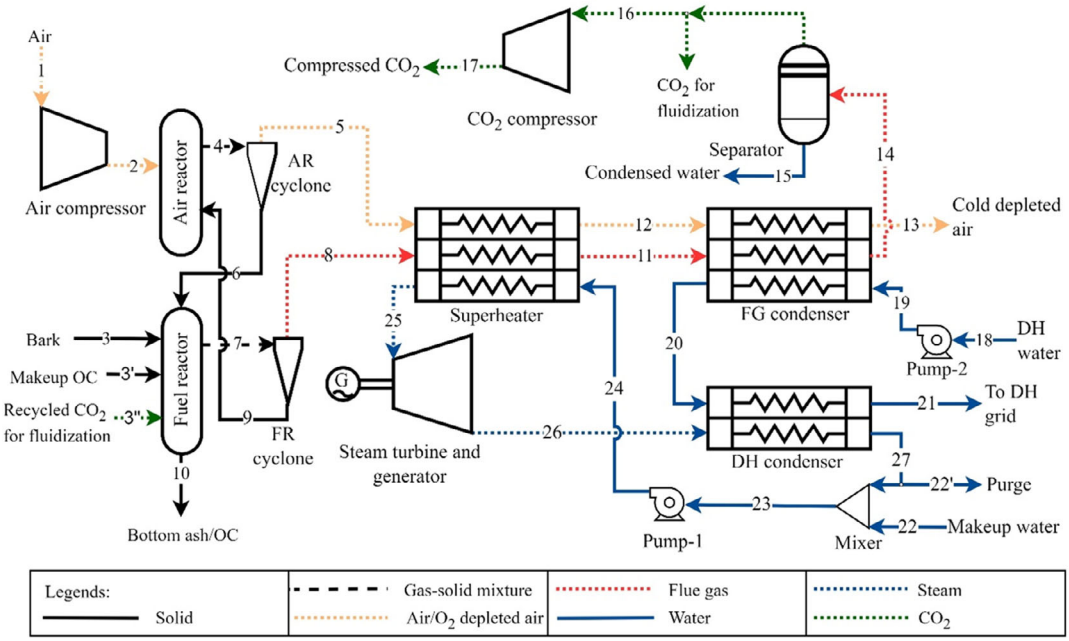

Figure 4. Simplified process flow diagram for CLC plant with CO_2 capture.

and LD slag is also performed to quantify the cost of exergetic destruction.

2.3.1. Energy and Exergy Analyses

The energy analysis provides the efficiency of energy utilization and can be used for evaluating electrical and energy efficiency. The exergy analysis provides information about the real performance of the individual as well as the overall process. More information on energy and exergy analyses is given in the previous work.[15] The following equations are used to assess the performance of the base, PCC, and CLC plants.

The overall electrical efficiency ($\eta_{\text{Gross/net}}$) and district heat energy efficiency (η_{DH}) are given in Equation (11) and (12).[15]

$$\eta_{\text{Gross/net}} = \frac{\dot{W}_{\text{Gross/net}}}{\dot{m}_{\text{b}} \times \text{LHV}_{\text{b}}} \tag{11}$$

$$\eta_{\text{H}} = \frac{\dot{Q}_{\text{DH}}}{\dot{m}_{\text{b}} \times \text{LHV}_{\text{b}}} \tag{12}$$

where, $\dot{W}$ is the electrical power generated from the plant (MW), LHV_{b} is the lower heating value of bark and $\dot{m}_{\text{b}}$ is the mass flow rate of fuel (kg s^{-1}).

The overall electrical exergy efficiency ($\varepsilon_{\text{Gross/net}}$) is defined as[15]

$$\varepsilon_{\text{Gross/net}} = \frac{\dot{W}_{\text{Gross/net}}}{\dot{m}_{\text{bark}} \times Ex_{\text{b}}} \tag{13}$$

where, Ex_{b} is the exergy of bark, which is calculated from the following equation.[49]

$$Ex_{\text{b}} = \text{LHV}_{\text{b}} \times \beta \tag{14}$$

$$\beta = 0.1519\frac{H}{C} + 0.0616\frac{O}{C} + 0.0429\frac{N}{C} + 1.0064 \tag{15}$$

where, H, C, O, and N are dry mass fractions of hydrogen, carbon, oxygen, nitrogen, and sulfur in fuel as given in Table 2.

The EXERGYFL property set is used in the Aspen Plus to evaluate the exergy flow of the individual stream[15,28] except for the bark feed and heat streams. The specific exergy of bark as given in Table 2 is used to calculate the exergy input to the plant. The district heat generated in this work is considered a heat stream. Therefore, the exergy of the heat transfer stream (E_{DH}) is defined as given below (simplified from the equation given in the literature[15])

$$\dot{E}_{\text{DH}} = (\dot{Q}_{\text{DH,out}} - \dot{Q}_{\text{DH,in}}) \times \left(1 - \frac{T_{\text{o}}}{T}\right) \tag{16}$$

where, $\dot{Q}_{\text{DH, in}}$ and $\dot{Q}_{\text{DH,out}}$ are the amount of district heat stream entering and leaving the power plant (MW), T_{o} is the reference environment temperature (K) and T is the working temperature (K).

Prior to the exergoeconomic analysis, the exergy analysis is carried out separately to assess the exergy balance, exergy destruction rate, and exergy efficiency of individual components. For simplicity, the exergy analysis also uses the concept of fuel-product definitions used in exergoeconomic analysis as per the SPECO method.[50] The imported net exergy of the individual component or overall system is denoted as fuel exergy and the net export of the individual component or overall system is denoted as product exergy.[48] Based on these definitions, the exergy balance equation for the overall system and component 'k' is expressed as follows[48]

Table 7. Simulation assumptions and operating conditions of proposed systems.

Component	Parameters and description	Aspen block type
CFB boiler	Base plant:[41]	RGibbs
	$P = 1.013$ bar, $T = 1846$ °C	
	CLC plant[15]	
	Air reactor: $T = 900$ °C, $P = 1.013$ bar	
	Fuel reactor: adiabatic, $P = 1.013$ bar	
Air compressor[15]	P: 1.06 bar	Compr
	Isentropic efficiency: 85%	
Superheater[41]	Cold stream outlet temperature: 540 °C	HeatX/MHeatX
FG condenser[41]	Hot stream outlet temperature: 40 °C	HeatX/MHeatX
DH condenser[41]	DH supply temperature: 93.30 °C	HeatX/MHeatX
	DH return temperature: 44 °C	
Steam turbine and generator[15]	Discharge pressure: 1.1 bar	Turbine
	Isentropic efficiency: 82%	
CO_2 compressor[15]	Discharge pressure: 110 bar	MCompr
	Isentropic efficiency: 85%	
Pumps	Pump-1 discharge pressure: 1.11 bar[41]	Pump
	Pump-2 discharge pressure: 107 bar[41]	
	Pump-3 discharge pressure: 2.00 bar[46]	
	Isentropic efficiency: 85%	
Absorber and stripper	See Table 4 and 5	RadFrac

$$\dot{E}_{\mathrm{F}} = \dot{E}_{\mathrm{P}} + \dot{E}_{\mathrm{D}} \tag{17}$$

$$\dot{E}_{\mathrm{F,k}} = \dot{E}_{\mathrm{P,k}} + \dot{E}_{\mathrm{D,k}} \tag{18}$$

Where, $\dot{E}_{\mathrm{P,k}}$, $\dot{E}_{\mathrm{F,k}}$ and $\dot{E}_{\mathrm{D,k}}$ represent the net product exergy, fuel exergy, and exergy destruction rate of the component k, respectively. The exergy efficiency (ε_{k}) and exergy destruction ratio ($y_{\mathrm{D,k}}$) of component k are given in Equation (19) and (20),[48] respectively.

$$\varepsilon_{\mathrm{k}} = \frac{\dot{E}_{\mathrm{P,k}}}{\dot{E}_{\mathrm{F,k}}} \tag{19}$$

$$y_{\mathrm{D,k}} = \frac{\dot{E}_{\mathrm{D,k}}}{\sum \dot{E}_{\mathrm{D,k}}} \tag{20}$$

2.3.2. Economic and Exergoeconomic Analyses

Like exergy analysis, a separate economic analysis is carried out prior to exergoeconomic analysis to calculate the cost of each component. In this work, the economic analysis is carried out according to the NETL guidelines for the technoeconomic assessment of power plants.[51] More information about this is given in previous work.[15]

The capital expenditure of a process is classified into total capital requirement (TCR) and operating and maintenance costs. The TCR is derived from the cost of all the equipment and other costs (cost of auxiliaries, installation, land, buildings, etc.). The cost of component k (C_{k}) is calculated as[15]

$$C_{\mathrm{k}} = \frac{\mathrm{CEPCI}_{2022}}{\mathrm{CEPCI}_{\mathrm{Ref}}} C_{\mathrm{k,ref}} \left(\frac{S_{\mathrm{k}}}{S_{\mathrm{k,Ref}}} \right)^{n} \tag{21}$$

where, $C_{\mathrm{k,ref}}$ and n are reference cost and scaling exponent of equipment k, S_{k} and $S_{\mathrm{k,Ref}}$ are cacapacities present and reference equipment, respectively. CEPCI_{2022} and $\mathrm{CEPCI}_{\mathrm{Ref}}$ are the Chemical Engineering Plant Cost Index for the year 2022 (785.9)[52] and for the reference year, respectively. The CEPCI, cost, and capacity of reference equipment are given in **Table 8**. The key assumptions for the estimation of economic analysis are given in **Table 9** and total capital investment cost calculation is given in **Table 10**. In this work, the economic analysis is performed as given by Farajollahi and Hossainpour.[53]

The economic assessment can be conducted to estimate either the levelized cost of electricity (LCOE) or the levelized cost of district heat (LCODH) produced. The choice between the cost of heat and the cost of electricity depends on the specific goals and nature of the energy system under consideration. In this work, it is assumed that the primary focus of the combined heat and power plants is to provide thermal energy for heating purposes in a district heating network. Therefore, the economic analysis of all the plants is performed to calculate the LCODH. The interplay between LCOE and LCODH is important in systems where both electricity and heat are produced, as the revenue from

Table 8. Parameters used for calculation of the cost of equipment.

Equipment	$C_{\mathrm{k,Ref}}$ [M \$ $^{-1}$]	$S_{\mathrm{k,Ref}}$	Size basis	n	Reference [year]	Ref.
CFB boiler (base plant)	268.73	300.00	Power generation [MW]	0.74	2011	[72]
Fuel reactor	2.15	280.50	Oxygen carrier flow rate [kg s^{-1}]	0.67	2016	[48]
Air reactor	0.63	59.40	Air mass flow rate [kg s^{-1}]	0.67	2016	[48]
Compressor	7.30	10.00	Power consumption [MW]	0.67	2019	[48]
Pumps	0.02	250.00	Volumetric flow rate [m^3 h^{-1}]	0.14	2019	[48]
Steam turbine	30.60	67.00	Power output [MW]	1.00	2008	[48]
Heat exchanger	1.64	57.20	Heat transferred [MW]	0.90	2014	[48]

Table 9. Key parameters and assumptions for evaluating economic indicators.

Parameter	Value/description	Reference
Base year	January 2022	–
VOM	2% of TCI	[15]
FOM	1% of TCI	[15]
Ilmenite cost	200 € t^{-1}	[60]
LD slag cost	10 € t^{-1}	[60]
MEA cost	981 € t^{-1}	[73]
Ilmenite lifetime	850 h	[74]
LD slag lifetime	200 h	[75]
Plant lifetime [*t*]	30 years	[48]
Interest rate [*i*]	9%	[48]
Annual plant operation	5300 h $year^{-1}$	[41]
Bark price	5.00 € t^{-1}	[76]
District heat cost	4.9 € GJ^{-1}	[41]
Selling cost of electricity	31.90 € GJ^{-1}	[41]

Table 10. Calculations for TCI.[53]

Parameter	Value
BEC	Sum of cost of equipment and installation cost
EPC contractor	17.5% BEC
EPCC	BEC + EPC
Process contingency	40% bec
Project contingency	20%]EPCC and process contingency]
TPC	EPCC + process and project contingency
Owner's cost	20% TPC
Total overnight cost	TPC + owner's cost
TCI	1.154 × overnight cost

electricity sales can influence the overall cost structure of providing district heat. The LCODH specifies a break-even cost for a unit district heat generation and is estimated as given in Equation (22) (modified from the equation given in the literature[54]).

$$\mathrm{LCODH} = \frac{\mathrm{ACC} + \mathrm{TOC} - \text{Annual plant revenue}}{\text{Annual district heat genration}} \tag{22}$$

where, ACC is the annual capital cost, which is a product of TCI and capital recovery factor (CRF) as given below[54]

$$\mathrm{ACC} = \mathrm{TCI} \times \mathrm{CRF} \tag{23}$$

The capital recovery factor to convert total plant cost into the annual cost is given below[54]

$$\mathrm{CRF} = \frac{i \times (i+1)^t}{(i+1)^t - 1} \tag{24}$$

where, t and i are the plant lifetime and interest rate as given in Table 9.

After estimating the levelized cost of district heat, a payback period of the plant is calculated to investigate the time of initial investment. The payback period is a ratio of total capital expenditure to annual plant profit. In this work, the plant revenue includes the district heat cost and electricity cost. The payback period and annual plant profit are calculated as[54]

$$\text{Payback period} = \frac{\mathrm{TCI}}{\text{Annual plant profit}} \tag{25}$$

$$\text{Annual plant profit} = \text{Annual plant revenue} - \mathrm{TOC} \tag{26}$$

The specific exergy costing method (SPECO) has been applied to quantify the cost of exergetic destruction of CLC-based DHP plants.[50] The general cost balance equation for a component k is presented in Equation (27). The cost balance, auxiliary, fuel, and product equations of the individual components of the CLC plant are listed in **Table 11**.

$$E_{\mathrm{F,k}} c_{\mathrm{F,k}} + Z_{\mathrm{k}} = E_{\mathrm{P,k}} c_{\mathrm{P,k}} \tag{27}$$

where, $c_{\mathrm{P,k}}$ and $c_{\mathrm{F,k}}$ are the cost per unit exergy of product and fuel, respectively. Z_{k} is a cost rate, which is represented below[48]

$$Z_{\mathrm{k}} = (\mathrm{TCI} \times \mathrm{CRF} + \mathrm{TOC}) \times \frac{C_{\mathrm{k}}}{t \times \sum C_{\mathrm{k}}} \tag{28}$$

where, TCI, TOC, and t are the total capital investment, total operating and maintenance cost, and annual operation of the plant.

Table 11. Fuels, products, cost balance, and auxiliary equations of the individual components.

Component	Fuel	Product	Cost balance equation	Auxiliary equation
Air compressor	W_{air}	E_2–E_1	$c_{\mathrm{air}} W_{\mathrm{air}} + c_1 E_1 + Z_{\mathrm{air}} = c_2 E_2$	$c_{\mathrm{air}} = 31.90$ € GJ^{-1}
CFB boiler	$E_2 + E_3$	$E_5 + E_8 + E_{10}$	$c_2 E_2 + c_3 E_3 + Z_{\mathrm{CFB}} = c_5 E_5 + c_8 E_8 + c_{10} E_{10}$	$c_5 = c_8 = c_{10}$, $c_{3'} = c_{3''} = 0$, $c_3 = 3.75$ € GJ^{-1}
Superheater	$(E_5$–$E_{12}) + (E_8$–$E_{11})$	E_{25}–E_{24}	$c_5 E_5 + c_8 E_8 + c_{24} E_{24} + Z_{\mathrm{Sup}} = c_{25} E_{25} + c_{11} E_{11} + c_{12} E_{12}$	$c_5 = c_{12}$, $c_8 = c_{11}$
FG condenser	$(E_{11}$–$E_{14}) + (E_{12}$–$E_{13})$	E_{20}–E_{19}	$c_{11} E_{11} + c_{12} E_{12} + c_{19} E_{19} + Z_{\mathrm{FG}} = c_{13} E_{13} + c_{14} E_{14} + c_{20} E_{20}$	$c_{11} = c_{14}$, $c_{12} = c_{13}$
DH condenser	E_{26}–E_{27}	E_{21}–E_{20}	$c_{20} E_{20} + c_{26} E_{26} + Z_{\mathrm{DH}} = c_{21} E_{21} + c_{27} E_{27}$	$c_{26} = c_{27}$
ST & generator	E_{25}–E_{26}	W_{ST}	$c_{25} E_{25} + Z_{\mathrm{ST}} = c_{26} E_{26} + c_{\mathrm{WST}} W_{\mathrm{ST}}$	$c_{25} = c_{26}$, $c_{\mathrm{ST}} = 31.90$ € GJ^{-1}
CO_2 compressor	W_{CO2}	E_{17}–E_{16}	$c_{\mathrm{CO2}} W_{\mathrm{CO2}} + c_{16} E_{16} + Z_{\mathrm{CO2}} = c_{17} E_{17}$	$c_{\mathrm{CO2}} = 31.90$ € GJ^{-1}
Pump-1	W_{P1}	E_{24}–E_{23}	$c_{\mathrm{WP1}} W_{\mathrm{P1}} + c_{23} E_{23} + Z_{\mathrm{P1}} = c_{24} E_{24}$	$c_{\mathrm{P1}} = 31.90$ € GJ^{-1}
Pump-2	W_{P2}	E_{19}–E_{18}	$c_{\mathrm{WP2}} W_{\mathrm{P2}} + c_{18} E_{18} + Z_{\mathrm{P2}} = c_{19} E_{19}$	$c_{\mathrm{P2}} = 31.90$ € GJ^{-1}

The cost associated with the productive component in the exergoeconomic analysis also includes the cost of exergy destruction. The cost of exergy destruction ($C_{D,k}$) is a product of cost of the fuel exergy ($c_{F,k}$) and exergy destruction of a component k ($E_{D,k}$), and it is expressed as[48]

$$C_{D,k} = E_{D,k} c_{F,k} \tag{29}$$

The exergoeconomic analysis is also performed to evaluate the relative cost difference in the component cost and exergoeconomic factor of a component. The relative cost difference (r_k), modified relative cost difference (r'_k), and exergoeconomic cost factor (f_k) of a component are given below[48]

$$r_k = \frac{C_{P,k} - c_{F,k}}{c_{F,k}} \tag{30}$$

$$r'_k = \frac{c_{P,k} - c_{F,k}}{c_{F,k}} \times \frac{C_k}{t \times \sum C_k} \tag{31}$$

$$f_k = \frac{Z_k}{c_{D,k} + Z_k} \tag{32}$$

The term f_k specifies which part cost needs to be reduced (Z_k or $C_{D,k}$). A higher value of f_k (>70%) means that reducing the investment cost and cost rate (Z_k) will be helpful to decrease the cost and improve the exergoeconomic performance). Practically, this is achieved by decreasing the purchasing cost of the unit and/or having a more efficient unit. A lower value of f_k (<30%) indicates that the cost of exergy destruction ($C_{D,k}$) needs to be reduced and its pragmatic solution augments the purchasing cost to improve the component exergy efficiency.[48] This practice will increase the product yield despite its being costly.

3. Results and Discussion

In this section, the base plant with DHP generation is first modeled and validated with the plant data available in the literature.[41] Then the CLC plant with DHP generation is modeled. Then the thermodynamic and economic analyses of the base plant, plant with PCC and CLC plant (using ilmenite and LD slag) are conducted. Further, the performance of CLC-based plants is investigated using exergoeconomic analysis.

3.1. Model Validation

As there is no direct experimental data on bark bark-fired CLC plants, the validation of the base plant is carried out. The Örtofta CHP plant connected to the district heat grid in Sweden modeled by Björnsson et al.[41] is considered a base plant. The comparison results of the present work and the literature work are outlined in **Table 12**. Model results showed a good agreement with the literature results with a maximum of 2.67% error. After the validation of the base plant, the conventional CFB boiler is replaced by air and fuel reactors of the CLC system (also referred to as the CFB boiler of the CLC plant). The validation results for the air and fuel reactors using iron oxide OC is given in **Table 13**.

3.2. Comparison of CLC Plant with Base Plant

Both the CLC plant cases are compared with each other and with the base plant. The comparison is made based on the energy, exergy, and economic analyses as given in the following subsections.

Table 12. Validation of base plant.

Sr. no.	Plant data	Literature work[41]	Present work	Error [%]
1	Fuel input [MW]	11 500	11 500	0.00
2	DH stream temperature after flue gas condensation [°C]	5370	5370	0.00
3	Air flow to the boiler [$m^3\ s^{-1}$]	3973	3959	0.35
4	Flue gas flow [$m^3\ s^{-1}$]	5078	4944	2.65
5	DH return temperature [°C]	4400	4400	0.00
6	DH supply temperature [°C]	9330	9350	−0.21
7	Steam pressure before turbine [bar]	10 700	10 700	0.00
8	Steam temperature before turbine [°C]	54 000	54 000	0.00
9	Steam flow to the turbine [$kg\ s^{-1}$]	3917	3930	−0.34
10	Net power generation [MW]	3303	3306	−0.07
11	DH power [MW]	9228	9199	0.31
12	Flue gas condenser heat duty [MW]	1802	1754	2.67
13	DH condenser heat duty [MW]	7426	7445	−0.26
14	Net electric efficiency [%]	2872	2874	−0.07
15	DH efficiency [%]	8024	7999	0.31
16	DH exergy [MW]	4876	4870	0.12
17	DH exergy efficiency [%]	4240	4235	0.12
18	Net plant efficiency [%]	7112	7109	0.04

Table 13. Validation of air and fuel reactors.

Parameter	Sikarwar et al.[24]			Present work		
	T [°C]	P [bar]	m [kg s^{-1}]	T [°C]	P [bar]	m [kg s^{-1}]
Air to AR	40.00	11.50	1.57	40.00	11.50	1.58
Reduced OC	1035.80	11.00	7.39	1035.00	11.00	7.40
Fuel to FR	60.00	1.01	0.14	60.00	1.01	0.14
Fresh OC to FR	33.00	1.01	0.36	33.00	1.01	0.36
Oxidized OC	1050.00	11.00	7.56	1050.00	11.00	7.55
Purge from CLC	1050.00	11.00	0.36	1050.00	11.00	0.36

3.2.1. Energy and Exergy Analyses

The base plant, plant with PCC, and CLC plant are simulated using the operating parameters given in Table 7. The overall performance of the base plant, plant with MEA-based post-combustion CO_2 capture, CLC plant using ilmenite, and CLC plant using LD slag are compared based on the energy and exergy analyses followed by unit-wise exergy analysis.

Table 14 shows the overall comparison of all the plants based on energy analysis. In this work, a constant fuel energy input of 30 MW_{th} to all the plants is assumed. As part of the energy from the plant is utilized in the CO_2 capture process, the ST power generation for the plant with PCC is less compared to that of the base plant. Moreover, the energy penalty is also observed in the district heat generation for the case of post-combustion CO_2 capture. The PCC has a net energy penalty of 7.13 MW with 0.18 kg s^{-1} of CO_2 emissions compared to the base plant with 2.30 kg s^{-1} of CO_2 emissions. The CLC plant with ilmenite OC has more electricity and district heat generation with ≈100% CO_2 capture efficiency (**Figure 5**) compared to the base plant without CO_2 capture. Since waste bark is used as a fuel for combustion, the net negative emissions is achieved. The negative emissions of 4.05×10^{07} kg per year can be achieved for chemical looping combustion plants (Table 14). The electricity and district heat generation of this plant is even more compared to the plant with PCC. The CLC plant with ilmenite OC has an 8.23 MW higher net energy output compared to the plant with PCC. The performance of the CLC plant with LD slag OC is poor compared to the CLC plant with the ilmenite OC. This is due to the ilmenite OC having a higher oxygen transport capacity than LD slag and therefore CLC plant with ilmenite is more efficient.[55]

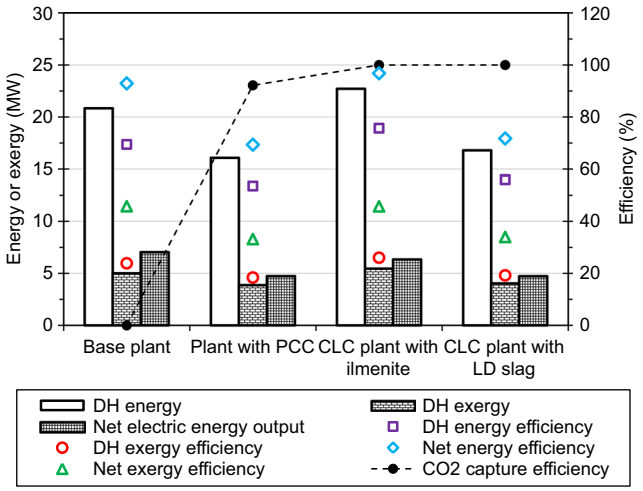

Figure 5. Overall performance comparison based on energy and exergy analyses.

Figure 5 represents the overall performance comparison for the base plant, plant with PCC and CLC plant based on both energy and exergy analyses. The net energy efficiency of a base plant, plant with PCC, CLC plant with ilmenite, and CLC plant with LD slag are 92.93%, 69.37%, 96.81%, and 71.76%, respectively. Integration of the CLC system not only benefits capturing ≈100% CO_2 over 92.18% for plant with PCC but also enhances net energy efficiency. The exergy of electric energy is the same as energy of electric energy, but the exergy of district heat is much less compared to its energy. This results in a reduction of overall efficiencies by 47.13%, 36.19%, 51.06%, and 37.77% for the base

Table 14. Overall performance comparison based on energy analysis.

Plant data	Unit	Base plant	Plant with PCC	CLC plant with ilmenite	CLC plant with LD slag
Fuel input [based on LHV]	MW	30.00	30.00	30.00	30.00
ST & generator power output	MW	7.34	5.85	7.59	5.90
Air compressor power consumption	MW	0.05	0.05	0.13	0.09
Auxiliary loss	MW	0.11	0.08	0.11	0.09
CO_2 compression power consumption	MW	0.00	0.86	0.87	0.87
Total power consumption	MW	0.16	1.00	1.11	1.05
Net electric energy output	MW	7.04	4.74	6.33	4.73
DH energy	MW	20.84	16.07	22.71	16.80
Net energy output	MW	27.88	20.81	29.04	21.53
CO_2 emitted from FR	kg s^{-1}	2.30	2.30	2.30	2.30
CO_2 captured	kg s^{-1}	0.00	2.12	2.30	2.30
CO_2 emitted	kg s^{-1}	2.30	0.18	0.00	0.00
Annual negative emissions	kg	0.00	4.05×10^{7}	4.37×10^{7}	4.37×10^{7}

plant, plant with PCC, CLC plant with ilmenite, and CLC plant with LD slag, respectively. The energy supplied to the district heating grid is assumed as a single heat stream in Aspen Plus software, and the exergy of this heat stream is evaluated using Equation (16). The overall exergy efficiency follows energy efficiency trends and as predicted, the highest net exergy efficiency is observed for the CLC plant using an ilmenite OC. Although the net electric efficiency of the CLC plant with LD slag OC is less than the plant with PCC, the net energy and exergy efficiencies are higher due to the more district heat generation.

In this work, a unit-wise exergy analysis is also carried out to identify the level of energy utilization in the plant. This also helps to identify the exergy destruction rates and the explanation for low efficient or high exergy destruction units. **Table 15** represents the exergy destruction and efficiency for the main components in the base plant, plant with PCC and CLC plant. To make the comparison straightforward, the air and fuel reactors along with their cyclone separators of the CLC plant are considered as one CFB boiler. Hence, the entering streams to the CFB boiler of the CLC system are stream numbers 2 and 3, whereas the leaving streams are stream numbers 5, 8, and 10 (see Figure 4).

The unit-wise exergy destruction in the plant is carried out as per Equation (18) and Table 11. For all the district heat and power generation cases, the largest exergetic destruction is observed in the CFB boiler followed by the superheater, steam turbine, and DH condenser (Table 15). The rest of the components in the plant have small exergy destruction. The CFB boiler of the base plant, plant with PCC, CLC plant using ilmenite, and CLC plant using LD slag accounts for about 54.71%, 48.59%, 68.91%, and 77.86% of total exergy destruction, respectively. Moreover, the CLC cases have more exergy destruction in the CFB boiler compared to the base plant. However, the total exergy destruction in the plant is more for the base plant and plant with PCC compared to the CLC plants. Among the two CLC cases, the mass flow rate of fresh OC and the circulated between the air and fuel reactor is higher for the LD slag case compared to that for the ilmenite case. The higher mass flow rates involved in the process directly affect the exergy flow of the streams involved in the process and result in more losses. Hence, the CLC with LD slag OC has more exergy destruction in the CFB boiler (15.34 MW) compared to the CLC with ilmenite OC (13.78 MW). Having more exergy losses in the CFB boiler makes it less exergy efficient. The exergy efficiency CFB boiler for both the base plant and plant with PCC is 64.58%, whereas the CLC with ilmenite and LD slag are 57.42% and 52.50%, respectively. The low exergy efficiency or high exergy destruction in the combustion process is also found in other studies reported in the literature.[15,24,34,35,48] The lower exergy efficiency for the CLC case compared to the base case could be due to complex CLC operation. The exergy efficiency of the CFB boiler of a CLC plant can be improved by using sensitivity analysis of the operating conditions of a plant such as: operating temperature, pressure, OC to fuel ratio, fluidizing agent to fuel ratio, etc. The pump-1 and CO_2 compressor also have low exergy efficiency compared to the other units, due to the involvement of workload to pump water and compress captured CO_2 to high pressure, respectively. As the exergy destruction of pump-1 is about 0.1 MW, the exergy loss can be assumed negligible as compared to the high exergy destruction units.

3.2.2. Economic Analysis

The economic analysis is applied to the base plant and plant with PCC as well as CLC plants to evaluate the capital investment, operating cost, profit, levelized cost of district heat, and payback period. The economic results are summarized in **Table 16**. The main issue with PCC technology is the huge amount of energy utilization and the cost of installation cost. Hence, the plant with PCC has more investment cost compared to the base plant. The composition of iron and titanium in the LD slag OC is lower when compared to the ilmenite ore, as indicated in Table 3. Therefore, CLC with LD slag case requires a higher mass of OC for the complete combustion of fuel in the fuel reactor.

Table 15. Unit-Wise exergy destruction and exergy efficiency.

Block	Exergy destruction [MW]				Exergy efficiency [%]			
	Base plant	Plant with PCC	CLC plant with ilmenite	CLC plant with LD slag	Base plant	Plant with PCC	CLC plant with ilmenite	CLC plant with LD slag
Air compressor	0.01	0.01	0.02	0.01	85.29	85.29	85.29	85.29
CFB boiler	11.39	11.39	13.78	15.34	64.58	64.58	57.42	52.50
Superheater	6.65	6.48	2.83	1.67	68.20	68.96	84.01	87.17
FG condenser	0.11	0.01	0.10	0.03	93.03	99.35	94.37	97.90
DH condenser	1.23	1.02	1.46	1.18	80.89	79.87	79.56	78.14
ST & generator	1.34	1.07	1.39	1.08	90.26	90.26	90.26	90.26
Pump 1	0.09	0.07	0.09	0.07	59.88	62.34	61.69	61.53
Pump 2	0.00	0.00	0.00	0.00	99.90	99.90	99.95	99.95
Pump 3	–	0.00	–	–	–	99.63	–	–
CO_2 compressor	–	0.38	0.32	0.32	–	53.93	63.10	63.21
Absorber	–	0.20	–	–	–	81.79	–	–
Stripper	–	2.19	–	–	–	60.52	–	–
Heat exchanger	–	0.64	–	–	–	84.24	–	–

Table 16. Economic indicators for all cases.

Plant	TCI [M € $^{-1}$]	ACC [M € year^{-1}]	TOC [M € year^{-1}]	DH [GJ year^{-1}]	Annual profit from electricity [M € year^{-1}]
Base plant	23.16	2.25	2.21	397 690.06	4.28
Plant with PCC	26.44	2.57	2.44	306 682.26	2.88
CLC plant with ilmenite	25.69	2.50	3.46	433 306.68	3.85
CLC plant with LD slag	26.88	2.62	2.29	320 495.77	2.88

The cost of a fuel reactor is estimated by the flow rate of the OC entering the reactor (Table 8). Therefore, the cost of the fuel reactor is higher for the CLC plant with LD slag compared to the one with ilmenite resulting in slightly higher capital investment for CLC with LD slag. The higher TCI for the CLC plant compared to the base plant is due to the higher cost of the CFB boiler used for the CLC plant (i.e., air and fuel reactor) than the cost of the conventional CFB boiler used in the base case. Moreover, an additional cost of a CO_2 compressor unit in the CLC plant and plant with PCC increases the total cost of equipment compared to the base plant without CO_2 capture. For the case without CO_2 capture, the total capital investment can be reduced, but not achieve negative CO_2 emissions and the social cost of carbon will be subtracted from the revenue. The social cost of carbon calculations for the power plants is given in the previous work of Surywanshi et al.[15]

Integration of the PCC process in the base plant not only reduces the electricity and district heat generation but also reduces the annual profit. The CLC with ilmenite has more electricity and district heat generation but the annual profit is less compared to the base plant without CO_2 capture, however, the annual profit is more than the plant with PCC. The CLC with LD slag has more district heat generation but the same annual profit compared to the plant with PCC.

The levelized cost is a fundamental calculation used for the preliminary evaluation of an energy-producing project. In addition, the payback period helps to estimate how long the plant takes to recover the initial investment. **Figure 6** shows the payback period and LCODH generation for a base plant, plant with PCC and CLC plants. The lowest capital investment and high electricity generation for the base plant result in the lowest LCODH with the lowest payback period. However, integration of PCC with the base plant significantly increases the district heating cost and the payback period. The CLC plant with ilmenite OC has the lowest LCODH and payback period among the plants with CO_2 capture. The district heat of CLC plants using ilmenite and LD slag is 29.91% and 9.12% less expensive, respectively, compared to the plant with PCC. The levelized cost of district heating given in the literature are 4.17 € GJ^{-1},[56] 11.39 € GJ^{-1},[57] 5.56,[58] and 4.83 € GJ^{-1}.[59] Hence, the DH cost for both the CLC cases is within the range given in the literature[41] with ilmenite-based plant being the most economical.

The payback period follows the same pattern as the levelized cost for all the plant. Among the plants with CO_2 capture, the CLC plant with ilmenite OC has the lowest payback period of less than 10 years (*see* Figure 6). In this work, the social cost of carbon or damage cost due to CO_2 emissions for the base plant or revenue from the negative emissions for CLC plant the is not

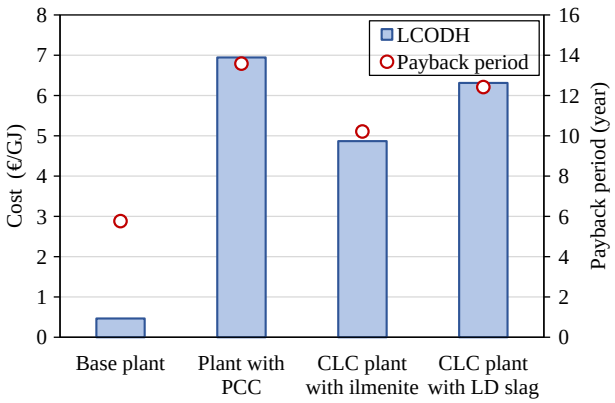

Figure 6. Levelized cost of district heat and plant payback period for all cases.

considered. If these costs are considered, the levelized cost for the base plant would be even more as mentioned in the literature.[15] The effect of the cost of both the OCs on the LCODH and payback period is also performed as the cost of the OC varies from location to location. **Figure 7** shows the effect of OC cost on LCODH and the payback period for the cost range given in the literature.[60] The LCODH and payback period were found to be increasing with the cost of OC for both cases. Moreover, better economic performance is observed for the ilmenite OC than the LD slag OC for the given range.

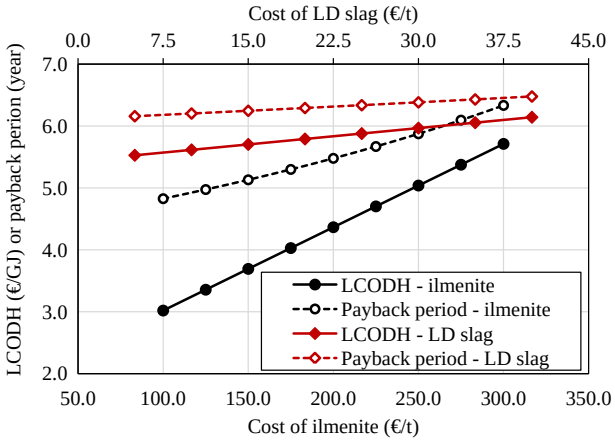

Figure 7. Effect of cost of ilmenite and LD slag on levelized cost of district heat and payback period of the plant.

3.3. Exergoeconomic Analysis

After performing thermodynamic and economic analysis, the exergy information of individual components is linked to the cost analysis. The combination of exergy and economic data helps to understand the performance of the component based on exergy and cost at the same time. The thermodynamic and economic analysis proved that the CLC technology for biomass-based DHP generation is the most favorable option compared to the post-combustion CO_2 capture DHP generation plant. Hence, the exergoeconomic analysis is carried out for the CLC plant alone. The results of the exergoeconomic components of the CLC plant using both OCs are summarized in **Table 17**. The cost rate (Z_k) and cost factor (f_k) distribution of the productive components are shown in **Figure 8** and **9**, respectively. The relative difference of the unit cost (r_k) and its modified cost (r'_k) are presented in **Figure 10**.

According to cost rate distribution, the most costly subsystem is ST & generator (35.29%), followed by CFB boiler (29.77%), CO_2 compressor (13.67%), and other subsystems (21.27%) for the CLC plant with ilmenite OC. Whereas, the most costly subsystem for the CLC with LD slag OC is the CFB boiler (44.83%), followed by ST & generator (26.19%), CO_2 compressor (13.08%), and other subsystems (15.91%).

As detailed in Section 3.2, the fuel reactor cost for the CLC plant using LD slag is higher than that for the ilmenite-based CLC plant, influencing the overall cost of the CFB boiler. Consequently, despite the ilmenite-based CLC plant having more expensive auxiliary units, the cost rate specifically for the CFB

Table 17. Exergoeconomic analysis results.

Component	Z_k [€ h^{-1}]	c_f [€ GJ^{-1}]	c_p [€ GJ^{-1}]	$E_{D,k}$ [GJ h^{-1}]	$C_{D,k}$ [€ h^{-1}]
CLC plant with ilmenite oxygen carrier					
Air compressor	43.38	31.74	144.49	0.07	2.21
CFB boiler	334.96	4.24	12.36	49.59	210.31
Superheater	101.14	11.82	13.15	10.19	120.47
FG condenser	15.14	3.85	6.47	0.38	1.46
DH condenser	75.07	11.03	17.54	5.25	57.97
ST & generator	397.05	9.26	18.61	4.99	46.23
Pump 1	1.88	14.41	26.87	0.33	4.79
Pump 2	2.69	0.02	0.62	0.00	0.00
CO_2 compressor	153.81	31.66	127.72	1.16	36.73
CLC plant with LD slag oxygen carrier					
Air compressor	27.15	31.74	131.45	0.05	1.58
CFB boiler	414.57	4.07	52.24	55.24	224.69
Superheater	62.50	14.04	14.41	6.03	84.63
FG condenser	6.85	3.27	4.92	0.09	0.30
DH condenser	47.18	13.40	21.81	4.24	56.76
ST & generator	242.16	10.92	18.61	3.88	42.33
Pump 1	1.42	14.46	26.93	0.26	3.76
Pump 2	2.03	0.02	0.63	0.00	0.00
CO_2 compressor	120.95	31.66	110.86	1.16	36.68

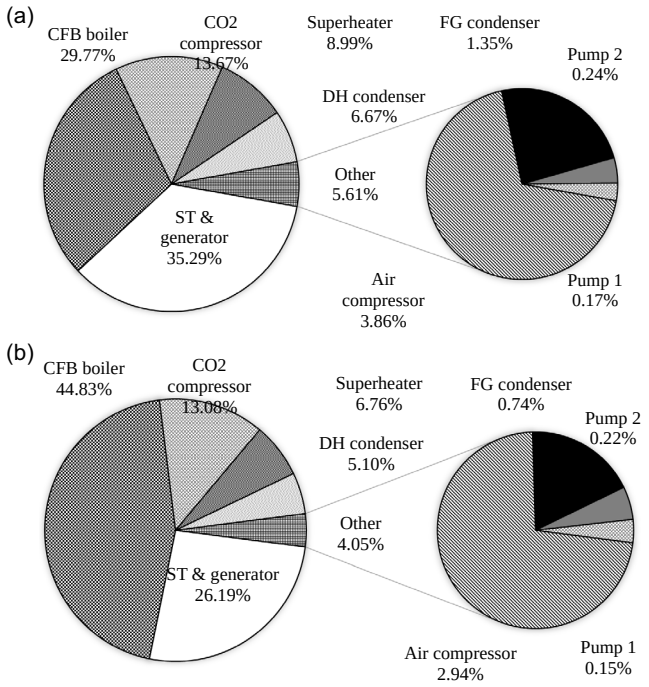

Figure 8. Cost rate (Z_k) distribution of individual components. a) CLC plant with ilmenite oxygen carrier. b) CLC plant with LD slag oxygen carrier.

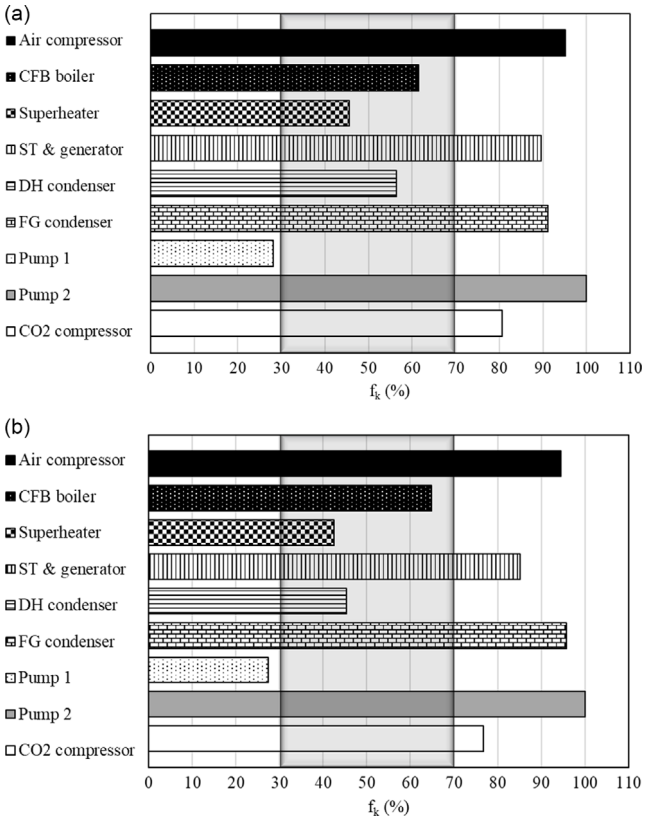

Figure 9. Cost factor distribution of individual components in the CLC plant. a) CLC plant with ilmenite oxygen carrier. b) CLC plant with LD slag oxygen carrier.

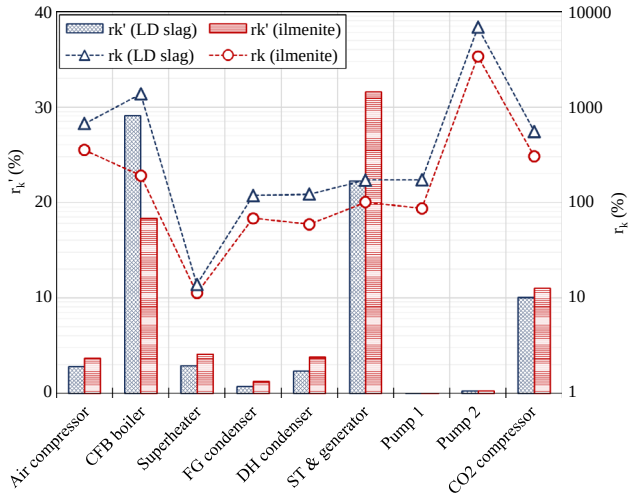

Figure 10. Relative cost distribution (r_k and r'_k) of the individual components of the CLC plant.

boiler in the LD slag-based CLC plant is higher than its ilmenite-based counterpart.

According to energy analysis, the CLC plant with ilmenite is more energy efficient, hence, it has a higher steam/water circulation rate, district heat, and electricity compared to the CLC plant with LD slag. Consequently, the components of the ilmenite-based plant, such as steam turbines, heat exchangers, and pumps, need to be larger in capacity. This results in an increased overall cost for these units in the ilmenite-based CLC plant when compared to the LD slag-based CLC plant, excluding the CFB boiler unit. As explained in Section 3.2, the cost of the fuel reactor of CLC with LD slag is higher than CLC with ilmenite, influencing the overall cost of the CFB boiler. Therefore, the cost rate (Z_k) for the CFB boiler of the CLC plant with LD slag is higher compared to the CLC plant with ilmenite.

The most vital subsystem from Table 17 is observed to be the CFB boiler as it has the highest magnitude of $C_{D,k} + Z_k$ (denominator of Equation (32), followed by a steam turbine, superheater, CO_2 compressor, and DH condenser due to their higher cost of exergetic destruction. On the contrary, the pump-1, pump-2, and FG condenser are the least important units as $C_{D,k} + Z_k$ is low. The ilmenite and LD slag OCs in the CLC system showed almost similar patterns for the exergoeconomic factor (f_k) except for some cost factors as explained previously. The cost factor (f_k) presented in Figure 9 represents whether the individual unit is cost-dominant or exergetic rate-dominant. The cost rate (Z_k) needs to be reduced if the exergoeconomic factor, f_k is higher than 70%, while the f_k lower than 30% indicates the cost of exergy destruction ($C_{D,k}$) needs to be reduced. This concept can increase the product yield despite its higher cost.[48] The exergoeconomic factor (f_k) for air compressor, steam turbine, FG condenser, pump-2, and CO_2 compressor exceeds 70%. This means that the cost rate (Z_k) must be reduced (which implies a reduction in the cost of the equipment). Practically, this is achieved by decreasing the purchasing cost of the unit. However, the $C_{D,k} + Z_k$ for pump-2, and FG condenser are low, hence, they are not a major concern. The exergoeconomic factor (f_k) is lower than 30% in pump-1, hence, reducing the cost of exergy destruction is inevitable. The pump-1 pressurize water from environmental condition to 107 bar pressure resulting in higher exergy destruction, but the amount of exergy destruction is not very high compared to the other unit (see Table 15). Moreover, the $C_{D,k} + Z_k$ of pump-1 is low, hence, it is not a major concern compared to the other units in the plant. The CFB boiler, superheater, and DH condenser have cost factors within the lower and upper limits, which indicates proper coordination between the cost of exergy destruction ($C_{D,k}$) and the cast rate (Z_k).

Another exergoeconomic factor, the relative difference in unit cost (r_k), reflects the connection between the exergoeconomic cost of unit fuel and product. The potential for improvement is greater when the system has larger r_k values. The term r_k only considers the relative cost reduction potential ($C_{D,k}$, and Z_k) from a position at the component level rather than the system level. Hence, the r_k value results in disagreement between reality and exergoeconomic analysis. The term modified r_k (or r'_k) considers both the product/fuel price difference of a unit and the contribution of component capital investment to the system. Hence, it shows the different cost reduction scenarios compared to the r_k.

From Figure 10, the CLC plant has an air compressor, CFB boiler, pump-2, and CO_2 compressor with a large value of r_k. These units have greater cost-reduction potential compared to the rest of the units in the plant. The CFB boiler of the LD slag-based CLC plant has a high r_k value compared to the ilmenite-based CLC plant. As mentioned before, the LD slag circulation flow rate is high compared to the ilmenite circulation flow rate in the CLC system. This results in more unit cost of fuel and product exergies and ends up with a large relative difference in cost. The r_k is evaluated based on $C_{D,k}$, and Z_k and disagrees with the reality. As an expel in this work, the pumps have high r_k signifying they have high-cost reduction potential. But, due to the low equipment cost, the cost reduction doesn't have a great influence on the whole plant. Hence, the r_k is modified to consider the unit cost of fuel and product and the capital investment. The highest modified relative difference of unit cost for the CLC plant with ilmenite is ST & generator unit (31.61%) followed by CFB boiler (18.29%), and CO_2 compressor (11.04%). However, the modified r_k for the CLC plant with LD slag is CFB boiler (29.07%) followed by ST & generator (22.29%), and CO_2 compressor (10.03%).

The disadvantage of this relative difference in the cost is that it does not specify what parameter, i.e., exergy destruction cost or cost rate to be reduced to have a better system. However, this information is available from the exergoeconomic cost fact (f_k). The exergoeconomic analysis reveals that more attention to be given to the CFB boiler, ST & generator, and CO2 compressor units of the CLC plant with both OCs to have a more exergoeconomically efficient system (**Table 18**).

4. Conclusions

In this work, a waste bark from the paper and pulp industry is considered as a prime energy input to the CLC plant, which is modeled for the two different OCs (ilmenite and LD slag) based on their cost. The CLC plant is compared with the base plant without CO_2 capture and the plant with post-combustion CO_2

Table 18. Nomenclature and abbreviations.

Nomenclature	
$\dot{m}$	Mass flow rate [kg s^{-1}]
C	Cost of equipment [M€]
c	Cost per unit exergy of a stream [€ GJ^{-1}]
E	Exergy flow [MW]
f	Exergoeconomic cost factor [%]
i	Interest rate [%]
n	Scaling factor
Q	Heat transfer [MW]
r	Relative cost difference factor [%]
r'	Modified relative cost difference factor [%]
S	Size of equipment
T	Temperature [°C]
t	Plant lifetime [years]
W	Work/power [MW]
y	Exergy destruction ratio [%]
Z	Cost rate [€ s^{-1}]
Abbreviations	
ACC	Annual capital cost
AR	Air reactor
BEC	Bare erected cost
BFPP	Bark fired power plant
CCS	Carbon capture and SEQUESTration
CDCL	Coal direct chemical looping
CEPCI	Chemical engineering plant cost index
CFB	Circulating fluidised bed
CLC	Chemical looping combustion
CLR	Chemical looping reformer
CPAQ0	Aqueous phase heat capacity at infinite dilution
CRF	Capital recovery factor
DA	Depleted air
DGAQFM	Aqueous free energy of formation at infinite dilution
DH	District heat
DHAQFM	Aqueous heat of formation at infinite dilution
DHP	District heat and power
EPC	Engineering and procurement cost
EPCC	Engineering, procurement, and construction cost
EU	Europe union
FG	Flue gas
FOM	Fixed operating and maintenance
FR	Fuel reactor
GHG	Greenhouse gas
iG	In-situ gasification
IGCC	Integrated gasification combined cycle
IMTP	Intalox metal tower packing
LCODH	Levelized cost of district heat
LCODH	Levelized cost of electricity
LHV	Lower heating value [MJ kg^{-1}]
MEA	Monoethanolamine
NETL	National energy technology laboratory
PCC	Post-combustion capture
ST	Steam turbine
TCI	Total capital investment
TCR	Total capital requirement
TOC	Total operating cost
TPC	Total plant cost
VOM	Variable operating cost
Subscripts/superscripts	
D	Destruction
F	Fuel
k	Component or unit
o	Reference environment
P	Product
Greek letters	
ε	Exergy efficiency [%]

capture. Comparative energy, exergy, economic, and exergoeconomic analyses are presented. The key conclusions of this work are given below. 1) Highest electricity (28.84 MW) and district heat (27.88 MW) are generated for base plat without CO_2 capture among all the plants. However, the CLC plant with ilmenite OC is found to be more energy and exergy-efficient among all CO_2 capture plants. 2) The CFB boiler unit (air and fuel reactor in the case of the CLC plant) contributes the highest amount of exergy destruction (50–80%) followed by the superheater (9–32%). 3) Among the plants with CO_2 capture to achieve negative emissions, the CLC plant with ilmenite has the lowest LCODH (4.58 € GJ^{-1}), and a payback period (9.69 years) followed by the CLC plant with LD slag (5.91 € GJ^{-1} and 11.84 years), and the plant with PCC (6.94 € GJ^{-1} and 13.58 years). 4) The LD slag circulation rate is higher compared to the ilmenite circulation rate resulting in the higher capacity and cost rate of the air and fuel reactors. 5) The exergoeconomic analysis concludes that the CFB boiler, ST & generator, and CO_2 compressor have more cost reduction potential and more attention to be given to these units, while other units are the least important. The analysis can be extended for components of CFB boiler with advanced equipment with chemical reactions as a part of future work.

Having poor performance of post-combustion CO_2 capture plants makes CLC plants more attractive for bark combustion to achieve negative CO_2 emissions. The present work concludes that for CO_2 capture, the CLC plant with ilmenite OC is the most favorable option based on energy, exergy, economic, and exergoeconomic analyses despite its high cost. Moreover, the plant has the potential to reduce CO_2 emissions efficiently.

Acknowledgements

This project was financed by the Chalmers Area of Advance Energy and J. Gust. Richert stiftelse.

Conflict of Interest

The authors declare no conflict of interest.

Data Availability Statement

The data that support the findings of this study are available from the corresponding author upon reasonable request.

Keywords

chemical looping combustion, district heat and power generation, economic analysis, exergoeconomic analysis

Received: May 29, 2023
Revised: October 31, 2023
Published online: December 16, 2023

[1] M. T. Johansson, S. Broberg, M. Ottosson, *J. Cleaner Prod.* **2021**, *311*, 127681.
[2] S. Karlsson, A. Eriksson, F. Normann, F. Johnsson, *Front. Energy Res.* **2021**, *9*, https://doi.org/10.3389/fenrg.2021.738791.
[3] Key Statistics 2020, European Pulp & Paper Industry, **2021**.
[4] Statista, Paper and Pulp Industry in Europe–Industries and Markets.
[5] J. Hansson, R. Hackl, M. Taljegard, S. Brynolf, M. Grahn, *Front. Energy Res.* **2017**, *5*, https://doi.org/10.3389/fenrg.2017.00004.
[6] IEA, World Energy Outlook 2017, Paris, France, **2017**.
[7] J. L. Míguez, J. Porteiro, F. Behrendt, D. Blanco, D. Patiño, A. Dieguez-Alonso, *Renew. Sustain. Energy Rev.* **2021**, *141*, 110502.
[8] Å Eliasson, E. Fahrman, M. Biermann, F. Normann, S. Harvey, *Int. J. Greenhouse Gas Control* **2022**, *118*, 103689.
[9] S. Werner, *Energy* **2017**, *126*, 419.
[10] J. Pelda, F. Stelter, S. Holler, *Energy* **2020**, *203*, 117812.
[11] P. Manz, K. Kermeli, U. Persson, M. Neuwirth, T. Fleiter, W. Crijns-graus, *Sustainability* **2021**, *13*, 1439.
[12] D. Connolly, H. Lund, B v. Mathiesen, S. Werner, B. Möller, U. Persson, et al., *Energy Policy* **2014**, *65*, 475.
[13] B. Möller, E. Wiechers, U. Persson, L. Grundahl, R. S. Lund, B. V. Mathiesen, *Energy* **2019**, *177*, 554.
[14] IEA, Energy Technology Perspectives 2020 – Special Report on Carbon Capture Utilisation and Storage, International Energy Agency **2020**, https://doi.org/10.1787/208b66f4-en.
[15] G. D. Surywanshi, B. B. K. Pillai, V. S. Patnaikuni, R. Vooradi, S. B. Anne, *Energy Convers. Manage.* **2019**, *200*, 112050.
[16] M. Finkenrath, Cost and Performance of Carbon Dioxide Capture from Power Generation, International Energy Agency, Paris, France **2011**.
[17] S. Vasudevan, S. Farooq, I. A. Karimi, M. Saeys, M. C. G. Quah, R. Agrawal, *Energy* **2016**, *103*, 709.
[18] K. Goto, K. Yogo, T. Higashii, *Appl. Energy* **2013**, *111*, 710.
[19] C. Song, Q. Liu, S. Deng, H. Li, Y. Kitamura, *Renew. Sustainable Energy Rev.* **2019**, *101*, 265.
[20] S. Jayanti, V. Saravanan, S. Sivaji *Proc. Inst. Mech. Eng., Part A* **2012**, *226*, 1003.
[21] K. E. Jenni, E. D. Baker, G. F. Nemet, *Int. J. Greenhouse Gas Control* **2013**, *12*, 136.
[22] A. Babin, C. Vaneeckhaute, M. C. Iliuta, *Biomass Bioenergy* **2021**, *146*, 105968.
[23] D. Mei, A. H. Soleimanisalim, A. Lyngfelt, H. Leion, C. Linderholm, T. Mattisson, *Chem. Eng. J.* **2022**, *433*, 133563.
[24] S. S. Sikarwar, G. D. Surywanshi, V. S. Patnaikuni, M. Kakunuri, R. Vooradi, *Renew. Energy* **2020**, *155*, 931.
[25] J. Adanez, A. Abad, F. Garcia-Labiano, P. Gayan, L. F. De Diego, *Prog. Energy Combust. Sci.* **2012**, *38*, 215.
[26] J. Adánez, A. Abad, T. Mendiara, P. Gayán, L. F. de Diego, F. García-Labiano, *Prog. Energy Combust. Sci.* **2018**, *65*, 6.
[27] G. D. Surywanshi, V. S. Patnaikuni, B. B. K. Pillai, S. B. Anne, R. Vooradi, *Int. J. Exergy* **2020**, *31*, 14.
[28] G. D. Surywanshi, V. S. Patnaikuni, R. Vooradi, S. B. Anne, *Energy* **2021**, *217*, 119418.
[29] J. Fan, L. Zhu, H. Hong, Q. Jiang, H. Jin, *Energy* **2017**, *119*, 1171.
[30] R. J. Thorne, E. A. Bouman, K. Sundseth, A. Aranda, T. Czakiert, J. M. Pacyna, M. Krauz, A. Celinska, *Int. J. Greenhouse Gas Control* **2019**, *86*, 101.
[31] V. Andersson, A. H. Soleimanisalim, X. Kong, F. Hildor, H. Leion, T. Mattisson, J. B. C. Pettersson, *Fuel Process. Technol.* **2021**, *217*, 106828.
[32] V. Andersson, A. H. Soleimanisalim, X. Kong, H. Leion, T. Mattisson, J. B. C. Pettersson, *Fuel Process. Technol.* **2022**, *227*, 107099.
[33] I. Gogolev, A. H. Soleimanisalim, D. Mei, A. Lyngfelt, *Energy Fuels* **2022**, *36*, 9551.
[34] O. J. Khaleel, F. Basim Ismail, T. Khalil Ibrahim, S. H. bin Abu Hassan, *Ain Shams Eng. J.* **2022**, *13*, 101640.
[35] R. Kumar, *Eng. Sci. Technol.* **2017**, *20*, 283.
[36] P. Zhao, *PhD Thesis*, **2015**.
[37] L. Sun, D. Wang, Y. Xie, *Energy Convers. Manage.* **2021**, *243*, 114400.
[38] A. Abusoglu, M. Kanoglu, *Renew. Sustain. Energy Rev.* **2009**, *13*, 2295.
[39] M. N. Khan, T. Shamim, *Int. J. Hydrogen Energy* **2017**, *42*, 4951.
[40] Aspentech. Aspen Tech v12.1 Software, Aspen Technology Inc **2023**.
[41] L. Björnsson, M. Pettersson, P. Börjesson, P. Ottosson, C. Gustavsson, *Sustain. Energy Technol. Assess.* **2021**, *48*, 101648.
[42] O. Condori, F. García-Labiano, L. F. de Diego, M. T. Izquierdo, A. Abad, J. Adánez, *Fuel Process. Technol.* **2021**, *222*, https://doi.org/10.1016/j.fuproc.2021.106963.
[43] Aspen Technology, Rate-Based Model of the CO_2 Capture Process by MEA using Aspen Plus, Aspen Technology Inc **2013**, pp. 1–25.
[44] G. Towler, R. Sinnott, in *Design*, Elsevier, Amsterdam **2008**.
[45] D. P. Hanak, C. Biliyok, H. Yeung, R. Białecki, *Fuel* **2014**, *134*, 126.
[46] H. Hikita, S. Asai, H. Ishikawa, M. Honda, *Chem. Eng. J.* **1977**, *13*, 7.
[47] M. Gustafsson, M. Rönnelid, L. Trygg, B. Karlsson, *Energy* **2016**, *111*, 341.
[48] Z. Sun, S. Wang, M. Aziz, *Energy Convers. Manage.* **2022**, *251*, 115013.
[49] Y. J. Zhao, Y. K. Zhang, Y. Cui, Y. Y. Duan, Y. Huang, G. Q., Wei, U. Mohamed, L. J. Shi, Q. Yi, W. Nimmo, *Energy* **2022**, *238*, https://doi.org/10.1016/j.energy.2021.121720.
[50] A. Lazzaretto, G. Tsatsaronis, *Energy* **2006**, *31*, 1257.
[51] A. Zeolle, M. J. Turner, V. Chou, Quality Guidelines for Energy System Studies: Introduction to Performing a Techno-Economic Analysis for Power Generation Plants, United states **2015**, https://doi.org/10.2172/1513273.
[52] Charles Maxwell. Cost Indices 2023. https://toweringskills.com/financial-analysis/cost-indices/ (accessed: January 2023).
[53] H. Farajollahi, S. Hossainpour, *Fuel Process. Technol.* **2022**, *231*, 107244.
[54] G. D. Surywanshi, V. S. Patnaikuni, R. Vooradi, M. Kakunuri, *Appl. Energy* **2021**, *304*, 117915.
[55] A. Hedayati, A. H. Soleimanisalim, T. Mattisson, A. Lyngfelt, *Fuel* **2022**, *313*, 122638.
[56] J. Beiron, F. Normann, F. Johnsson, *Int. J. Greenhouse Gas Control* **2022**, *118*, 103684.

[57] A. Egüez, *Util. Policy* **2021**, *72*, https://doi.org/10.1016/j.jup.2021.101252.
[58] K. Lygnerud, J. Ottosson, J. Kensby, L. Johansson, *Energy* **2021**, *234*, 121202.
[59] A. Pesola, *Energy* **2023**, *281*, 128241.
[60] F. Störner, F. Lind, M. Rydén, *Appl. Sci.* **2021**, *11*, 7935.
[61] N. M. A. Al Lagtah, S. A. Onaizi, A. B. Albadarin, F. A. Ghaith, M. I. Nour, *J. Environ. Chem. Eng.* **2019**, *7*, 103471.
[62] F. Li, J. Kang, Y. Song, J. Feng, W. Li, *Energy* **2020**, *194*, 116830.
[63] W. Xiang, S. Chen, Z. Xue, X. Sun, *Int. J. Hydrogen Energy* **2010**, *35*, 8580.
[64] S. Mukherjee, P. Kumar, A. Yang, P. Fennell, *J. Environ. Chem. Eng.* **2015**, *3*, 2104.
[65] J. Fan, H. Hong, L. Zhu, Z. Wang, H. Jin, *Energy Convers. Manage.* **2017**, *135*, 200.
[66] J. Fan, H. Hong, H. Jin, *Renew. Energy* **2018**, *125*, 260.
[67] Z. Shen, Z. Huang, *Chin. J. Chem. Eng.* **2018**, *26*, 2368.
[68] N. Mishra, B. Bhui, P. Vairakannu, *Energy* **2019**, *169*, 305.
[69] H. Shijaz, Y. Attada, V. S. Patnaikuni, R. Vooradi, S. B. Anne, *Energy Convers. Manage* **2017**, *151*, 414.
[70] E. Kurkela, M. Kurkela, I. Hiltunen, *Environ. Prog. Sustainable Energy* **2014**, *33*, 676.
[71] D. R. Zozulya, K. Kullerud, E. Ribacki, U. Altenberger, M. Sudo, Y. E. Savchenko, *Minerals* **2020**, *10*, 1029.
[72] Z. Guo, Q. Wang, M. Fang, Z. Luo, K. Cen, *Appl. Energy* **2014**, *113*, 1301.
[73] B. Keivani, A. Gungor, *J. CO2 Util.* **2022**, *62*, 102103.
[74] O. Condori, F. García-Labiano, L. F. de Diego, M. T. Izquierdo, A. Abad, J. Adánez, *Chem. Eng. J.* **2021**, *405*, 126679.
[75] F. Hildor, T. Mattisson, H. Leion, C. Linderholm, M. Rydén, *Int. J. Greenhouse Gas Control* **2019**, *88*, 321.
[76] J. M. Ahlström, A. Alamia, A. Larsson, C. Breitholtz, S. Harvey, H. Thunman, *Int. J. Energy Res.* **2019**, *43*, 1171.